

Urban1960SatSeg: Unsupervised Semantic Segmentation of Mid-20th century Urban Landscapes with Satellite Imageries

Tianxiang Hao*
Fudan University
Shanghai, China

Lixian Zhang*[†]
National supercomputing center in
Shenzhen
Shenzhen, China

Yingjia Zhang*
New York University Shanghai
Shanghai, China

Mengxuan Chen, Jinxiao Zhang
Tsinghua University
Beijing, China

Haohuan Fu[†]
Tsinghua University
Beijing, China

Abstract

Historical satellite imagery, such as mid-20th century Keyhole data, offers rare insights into understanding early urban development and long-term transformation. However, severe quality degradation (e.g., distortion, misalignment, and spectral scarcity) and annotation absence have long hindered semantic segmentation on such historical RS imagery. To bridge this gap and enhance understanding of urban development, we introduce **Urban1960SatBench**, an annotated segmentation dataset based on historical satellite imagery with the earliest observation time among all existing segmentation datasets, along with a benchmark framework for unsupervised segmentation tasks, **Urban1960SatUSM**. First, **Urban1960SatBench** serves as a novel, expertly annotated semantic segmentation dataset built on mid-20th century Keyhole imagery, covering 1,240 km² and key urban classes (buildings, roads, farmland, water). As the earliest segmentation dataset of its kind, it provides a pioneering benchmark for historical urban understanding. Second, **Urban1960SatUSM** (Unsupervised Segmentation Model) is a novel unsupervised semantic segmentation framework for historical RS imagery. It employs a confidence-aware alignment mechanism and focal-confidence loss based on a self-supervised learning architecture, which generates robust pseudo-labels and adaptively prioritizes prediction difficulty and label reliability to improve unsupervised segmentation on noisy historical data without manual supervision. Experiments show Urban1960SatUSM significantly outperforms existing unsupervised segmentation methods on Urban1960SatSeg for segmenting historical urban scenes, promising in paving the way for quantitative studies of long-term urban change using modern computer vision. Our benchmark and supplementary material are available at <https://github.com/Tianxiang-Hao/Urban1960SatSeg>.

CCS Concepts

• Computing methodologies → Image segmentation.

Keywords

Historical Remote sensing images, Benchmark of land use classification, Unsupervised learning in semantic segmentation

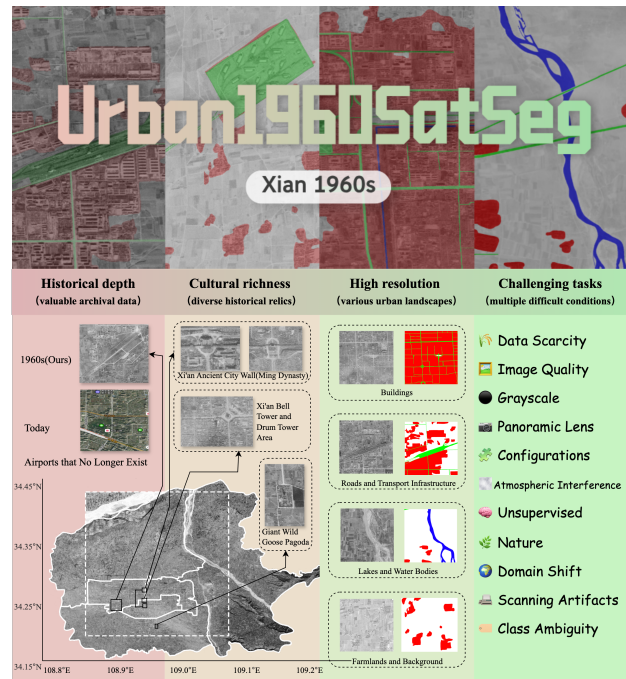


Figure 1: Overview of the Urban1960SatBench benchmark. Urban1960SatBench features four key properties: 1) Historical depth; 2) Cultural richness; 3) High resolution; 4) Challenging tasks.

1 Introduction

The pursuit of sustainable urban development, a cornerstone of global agendas such as the Sustainable Development Goals (SDGs) [31] and broader urban sustainability initiatives [37], necessitates a profound understanding of historical urban morphology. Analyzing past planning paradigms, infrastructure evolution, and land-use transitions in contemporary megacities provides crucial insights for addressing challenges related to urban equity, resilience, and environmental sustainability. Earth observation (EO) data from

*All authors contributed equally to this research.

[†]The corresponding author.

satellites offers an unparalleled opportunity to quantitatively assess urban systems across extensive spatial and temporal scales [39, 40].

Despite their immense potential for reconstructing long-term urban trajectories, satellite images from the mid-20th century remain largely underutilized. This under-exploration stems from two fundamental and interrelated challenges:

First, there is an acute lack of large-scale, meticulously curated benchmark datasets specifically designed for historical remote sensing data. Unlike modern imagery, historical archives are characterized by inherent degradations, including significant geometric distortions, limited spectral and spatial resolution, and a pronounced scarcity of ground truth annotations. These unique properties render existing contemporary benchmarks structurally incompatible [23, 36]. For instance, Keyhole reconnaissance data, a primary source of mid-century imagery, presents intrinsic degradations that severely impede both algorithmic interpretation and manual labeling. These include: i) a grayscale-only format, ii) spatial resolutions varying between 0.6 and 1.8 meters, and iii) severe geometric distortions, scanning artifacts, and poor contrast. Such characteristics not only obfuscate visual semantics but also render high-fidelity annotation exceptionally burdensome and ambiguous, particularly in the absence of concurrent reference data. The substantial cost and inherent ambiguity associated with large-scale manual labeling make supervised learning approaches largely infeasible, underscoring the urgent need for alternative strategies to curate and leverage these invaluable historical resources.

Second, there is a concurrent absence of scalable analytical methods specifically engineered to overcome the aforementioned data degradations. Modern deep learning approaches, while powerful, are heavily reliant on vast annotated corpora. The stark domain shift between mid-century and contemporary satellite imagery, encompassing differences in sensor modality (grayscale vs. multi-spectral), reflectance properties, architectural patterns, and various degradations, significantly limits the transferability of existing deep learning models. This often leads to semantic misalignment and representational collapse when applied to historical data. Consequently, in the pervasive absence of sufficient ground-truth data, conventional supervised methods become untenable. This critical gap necessitates the development of novel, unsupervised segmentation strategies capable of extracting semantics from spectrally impoverished, noisy, and distorted inputs, which is essential for enabling large-scale, quantitative analysis of early urban forms.

To address this, we introduce **Urban1960SatSeg**, a novel framework designed for the unsupervised extraction of historically dormant urban areas from Keyhole satellite imagery. As presented in Fig. 1, Urban1960SatSeg consists of: (i) **Urban1960SatBench**, the earliest-time semantic segmentation dataset among all existing remote sensing benchmarks, and (ii) **Urban1960SatUSM**, a robust model for unsupervised segmentation.

Urban1960SatBench is the first professionally annotated semantic segmentation dataset derived from mid-20th-century declassified Keyhole satellite imagery. This dataset, initially covering over 1,240 km² of Xi’an, China, provides meticulously curated multi-class land use and binary impervious surface products. Its construction, involving expert interpretation and cross-referencing with extensive archival materials, represents a significant technical and logistical

advancement, enabling quantitative analysis of historical urban development previously hindered by data scarcity.

To fully leverage Urban1960SatBench, the Urban1960SatUSM is proposed as a novel unsupervised segmentation method engineered to overcome the methodological barriers associated with historical satellite imagery. Urban1960SatUSM integrates the Segment Anything Model (SAM) for initial pseudo-label generation with a dual-branch DINO-based self-supervised learning architecture. The key contributions include a confidence-aware alignment mechanism that transforms diverse zero-shot masks from the SAM into reliable pseudo-labels and Focal-Confidence Loss that integrates class-level prediction difficulty and pixel-level label reliability to precisely focus learning on trustworthy and semantically challenging regions, leading to significantly improved unsupervised segmentation of historical imagery without additional manual annotation.

In summary, our contributions are threefold: 1) We introduce **Urban1960SatBench**, the first semantic segmentation dataset covering mid-20th-century grayscale satellite imagery, enabling urban land use and impervious surface analysis under grayscale degradation. 2) We propose **Urban1960SatUSM**, a novel framework for unsupervised segmentation and classification of historical satellite imagery that reduces the dependence on manual annotation. 3) Experimental results demonstrate that Urban1960SatUSM outperforms five DINO-based self-supervised approaches and several classical unsupervised baselines, underscoring its effectiveness in high-resolution Keyhole image segmentation and its potential to enhance interpretability in historical remote sensing analysis.

2 Related Work

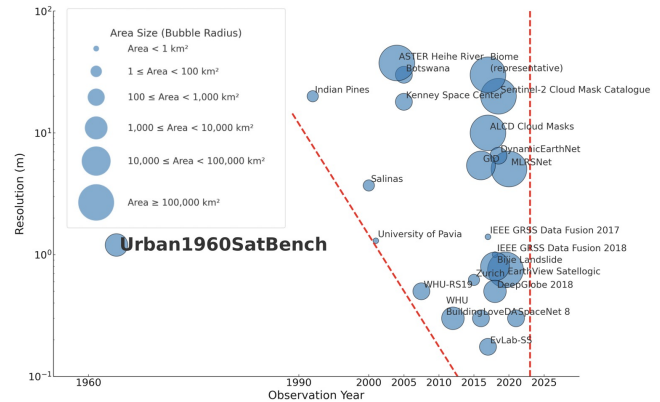


Figure 2: Visualization of high-resolution remote sensing segmentation datasets by year, resolution, and coverage. More recent datasets show greater diversity in resolution and extent, while Urban1960SatBench is the earliest with relatively high resolution, bridging a key temporal gap.

2.1 Segmentation datasets in Remote Sensing

Segmentation datasets are fundamental for advancing remote sensing applications. We systematically review the existing datasets in remote sensing segmentation (detailed in Tab. 1). It is clear to observe a distinct and problematic evolutionary trajectory that while

Table 1: Comparative Analysis of Leading High-Resolution Satellite Sensor Image Segmentation Benchmarks.

Dataset	Resolution (m)	Observation Year	Area (km ²)
EarthView Satellogic[2]	0.5 to 1	2017–2022	About 437,682
SpaceNet 8[15]	0.3	2021	850
MLRSNet[24]	0.1 to 10	2020	About 360,000
95-Cloud[21]	30	2019	34,225
ALCD Cloud Masks[10]	10	2016–2018	About 320,000
Sentinel-2 Cloud Mask Catalogue[9]	20	2018–2019	About 214,500
DynamicEarthNet[29]	3 to 10	2018–2019	About 708
IEEE GRSS Data Fusion 2018[19]	1	2018	-
DeepGlobe 2018[7]	0.5	2018	2220
Bijie Landslide[17]	0.8	2018	About 38,000
SEN12MS[26]	10 to 50	2018	About 1,184,846
IEEE GRSS Data Fusion 2017[27]	1.4	2017	-
Biome[8]	30	2017	About 2,987,000
EvLab-SS[41]	0.1 to 0.25	2017	About 720
SPARCS Validation[32][14]	30	2016	About 72,000
LoveDA[34]	0.3	2016	536.15
Zurich Summer[33]	0.62	2015	9.37
GID[30]	0.8 to 10	2014–2018	75,900
WHU Building Dataset[16]	0.3	2012	1000
WHU-RS19[35][4]	0.5	2005–2010	130
Kenney Space Center[6]	18	2005	101.94
Botswana[6]	30	2005	340.07
ASTER Heihe River[1]	15 to 60	2000–2008	143,000
University of Pavia[6]	1.3	2001	0.35
Pavia Centre[6]	1.3	2001	1.32
Salinas[6]	3.7	Around 2000 (1990–2010)	1.52
Indian Pines[6]	20	1992	8.41
Urban1960SatBench	0.6 to 1.8	1960s	1240

recent years have witnessed a proliferation of datasets characterized by impressive diversity in spatial resolutions and expansive geographic coverage, a fundamental limitation persists in their temporal depth. As depicted in Fig. 2, the prevailing trend strongly favors contemporary imagery, often capturing sub-meter to few-meter details of present-day land cover. Conversely, datasets extending into earlier periods, particularly those preceding the satellite era’s mature stages (e.g., 1990s - 2010s), exhibit significantly coarser spatial resolutions and constrained geographic extents. This disparity largely stems from historical sensor capabilities, the complexities of analog data acquisition, and the challenges of large-scale digitization and georeferencing. This pronounced historical data gap [23, 36] critically impedes granular, long-term urban change analysis, which is vital for understanding historical development trajectories, assessing the efficacy of past planning policies, and informing future sustainability strategies. Addressing this temporal discontinuity is therefore paramount for a holistic understanding of global urban evolution.

The Urban1960SatBench dataset directly addresses this critical gap. The Urban1960SatBench is the first pixel-level segmentation dataset derived from high-resolution, 1960s grayscale imagery, covering an expansive over 1,000 km². Beyond its inherent value for remote sensing and social science, Urban1960SatBench provides historical high-resolution imagery with comprehensive multi-label annotations to support land-use changes and sustainable development research, establishing a crucial benchmark for evaluating unsupervised semantic segmentation models in historically degraded contexts.

2.2 Segmentation model in Remote Sensing

Remote sensing image segmentation often has several challenging features such as severe imbalance in foreground and background

distribution, complex background, intra-class heterogeneity, inter-class homogeneity and tiny objects[13]. These challenges are intensified in our task due to grayscale inputs, variable resolution, and historical image degradation. Most segmentation models use CNN or Transformer-based architectures. A method is proposed for the single-target segmentation task, where the existing segmentation performance of Large SAM is leveraged by freezing its parameters, while a Small model generates boxes prompts, to assist SAM in achieving accurate segmentation of urban villages from satellite images [42]. For the semantic segmentation task of remote sensing images, a simple and effective framework is proposed that uses the objects and boundaries generated by the SAM and assists model training by designing object consistency loss and boundary preservation loss[20].

2.3 Unsupervised semantic segmentation in computer vision

Semantic segmentation based on deep learning often utilizes encoder-decoder architectures for pixel-wise classification [43]. The existing researchers have explored various prompt mechanisms by designing unique decoders equipped with multiple prompt recognition features and task-specific functions, achieving notable performance in zero-shot semantic segmentation [45][44][38]. From an unsupervised learning perspective, a common approach involves two key steps: the generation of pseudo masks and the subsequent training of models using these automatically derived labels. For example, STEGO [12] proposes a method that combines clustering and Conditional Random Field (CRF) refinement to perform knowledge distillation by leveraging the inherent correlations within self-supervised features. Another approach, HP [28], contributes to mine global and local hidden positive samples, achieving performance improvements through contrastive learning. Additionally, Primaps [11] utilizes the intrinsic properties of self-supervised learning features to construct pseudo labels, ultimately leading to unsupervised semantic segmentation. However, most methods fail under grayscale, heavily degraded data as historical RS images. Urban1960SatUSM addresses this gap with a framework tailored to such conditions.

3 Urban1960SatBench Dataset

Urban1960SatBench is a high-fidelity, city-scale semantic segmentation benchmark derived from declassified 1964 Keyhole (KH-4A) panchromatic satellite imagery [5] co-registered with the 1965 official Xi’an urban distribution map. Through rigorous geo-referencing and expert manual annotation, the dataset provides pixel-level labels for impervious surfaces and four urban land-use categories (roads, buildings, water bodies and other urban types). Xi’an, as one of China’s oldest capitals, exhibits a unique juxtaposition of millennia-old cultural heritage and modern urbanization pressures. Consequently, Urban1960SatBench not only pioneers historical urban analysis using reconnaissance imagery but also establishes a challenging domain for segmentation models, owing to grayscale distortions and limited spatial resolution. This dataset facilitates studies in historical urban morphology reconstruction, cultural heritage conservation, and cross-temporal model generalization, offering a foundational resource for both Remote Sensing (RS) and

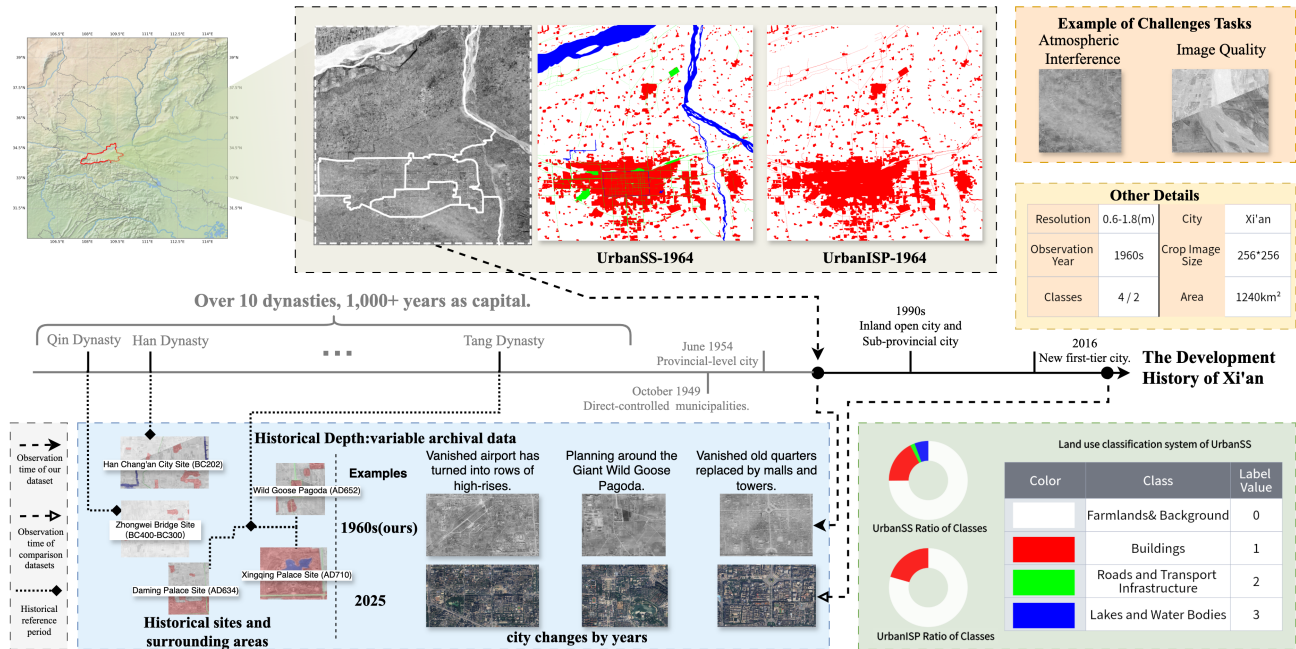


Figure 3: Urban1960SatBench, highlighting its spatial structure, task-specific challenges, semantic category design, and value for historical cross-era urban dynamics research.

Computer Vision (CV) communities. The complete dataset (images, masks, ISP masks, metadata, and baseline scripts) along with detailed information is publicly available under a Creative Commons Attribution-NonCommercial license at <https://github.com/Tianxiang-Hao/Urban1960SatSeg>.

3.1 Dataset Construction

Data Area: Urban1960SatBench covers Xi'an, one of China's ancient capitals, which has served as the political, economic, and cultural center for over a dozen dynasties, including the Western Zhou, Qin, Western Han, Sui, and Tang, with a cumulative capital history spanning more than a millennium. In contemporary times, Xi'an remains a strategic hub for Northwest China's economic development and a focal point of national initiatives such as the Belt and Road. Rapid urbanization in the late 20th and early 21st centuries has introduced significant development pressures, necessitating a careful balance between modernization and preservation of cultural heritage, making it an exemplary case for remote sensing-based studies of urban growth, heritage conservation, and morphological evolution.

Data Acquisition: Remote sensing imagery was acquired in 1964 by the U.S. KH-4A Keyhole reconnaissance satellite and declassified in recent decades, equipped with a panoramic camera featuring a focal length with an effective ground sampling distance (GSD) of approximately 0.6 m/pixel in the city center and approximately 1.8 m/pixel in the sub-urban area, capturing panchromatic film at nadir with film digitization at 12 bits depth.

Radiometric and Geometric Preprocessing: Original film scans underwent histogram matching, control-point-based geo-referencing,

Rational Polynomial Coefficients (RPC) refinement for abnormal brightness reduction, fine geospatial registration, relief displacement correction, and contrast variations reduction across overlapping frames. Please refer to the supplementary material for more details.

Annotation: Subsequent to radiometric and geometric preprocessing, remote sensing specialists annotated the dataset using comparative analysis between Keyhole satellite imagery and the 1965 urban map derived from the Department of Shaanxi Provincial Archives. Remote sensing specialists with high historical imagery interpretation experience performed manual annotation with a final pass to ensure topological consistency and verifying that major landmarks (e.g., cultural heritage) align correctly. Annotations are produced in two formats: impervious surface product (ISP) and urban land use classification. The latter adheres to standard remote sensing classification categories[25], including roads and transportation facilities, buildings, water bodies, green spaces, farmland, and other urban-use types, serving as a valuable reference for urban development analysis in China and globally during the 1960s.

3.2 Dataset Exploration

Overview: As shown in Fig. 3, Urban1960SatBench is currently a city-level urban landcover segmentation dataset for demonstration. The dataset consists of two products: (1)**UrbanISP-1964**: the Urban1960SatISP impervious surface product; (2)**UrbanSS-1964**: the Urban1960SatSS semantic segmentation product for urban landcover. The UrbanISP-1964 and UrbanSS-1964 subsets are divided into training, validation, and testing sets, consisting of 614, 154, and 256 image-label pairs, respectively.

Highlights: We summarize the key features of Urban1960SatBench as follows: (1) **Pioneering Benchmark:** Urban1960SatBench is the first segmentation benchmark built on 1960s Keyhole imagery, enabling historical urban analysis and zero-shot generalization across cities and decades, promoting advancements in both remote sensing (RS) and computer vision (CV) communities. (2) **Challenging Conditions:** Urban1960SatBench contains the inherent complexities of historical remote sensing imagery, including grayscale imaging, geometric distortions, and resolution limitations. These challenges demand models with strong generalization in unsupervised settings, making Urban1960SatBench more difficult than most modern benchmarks. (3) **Comprehensive Urban Landscape Coverage:** Urban1960SatBench captures diverse urban features and land cover types in a historically significant Chinese city. It includes detailed urban elements such as roads, buildings, water bodies, green areas, and farmland, all of which are manually annotated by domain experts. This provides a valuable resource for the analysis of historical urban form, planning trends, and socio-economic landscapes within the broader context of global urban studies.

4 Urban1960SatUSM

As shown in Fig. 4, we design a three-stage framework for unsupervised segmentation on historical imagery: pre-pseudo-label generation, self-supervised learning, and loss computation. Initially, the SAM generates region-level masks from unlabeled images via grid-based prompts, which are aggregated into complete pseudo-label maps. In parallel, a frozen DINO-based dual-branch network extracts patch-level features, with the teacher updated via EMA. SAM and teacher outputs are compared with the student’s predictions to compute consistency-aware supervision and a confidence map, which are fused via a novel focal-confidence loss, which adaptively emphasizes reliable and semantically challenging regions.

4.1 Pre-Pseudo-Label Generation and Self-Supervised Learning Framework

In this stage, segmentation masks are generated using the SAM under prompt guidance. The input image is processed to extract spatially distributed points as prompt locations. For each, SAM generates a binary mask for the most salient instance. These individual masks are then merged to form an initial segmentation output. To address spatial coverage issues, a filling operation assigns pseudo-labels to unmarked regions, followed by skeleton-based width division to refine structures. This process yields a full-resolution segmentation prior which, despite containing noise and class ambiguity, provides structural guidance for downstream feature learning.

To efficiently learn meaningful representations from unlabeled data, we adopt the dual-branch DINO framework and segmentation head module from Primaps-EM [11]. The architecture uses a momentum-updated teacher and a trainable student, receiving two augmented views of the same image. Both encoders extract patch-level features that are projected into a shared embedding space and clustered to produce semantic predictions. The teacher parameters are updated via the exponential moving average (EMA) of the student’s weights to maintain a stable learning signal. The dual-branch structure, guided by SAM priors, enables robust semantic

learning despite low-level noise and missing supervision—critical in historical imagery.

4.2 Pseudo-Label and Student Loss

The student network is supervised by comparing its predictions with those from the teacher model and the SAM-derived pseudo-labels. Specifically, the SAM pseudo-labels and teacher predictions are reshaped into patch-level representations and aligned with the student’s outputs. A consistency loss is computed to encourage agreement among these three sources. To robustly guide learning in the presence of noisy or uncertain supervision, we introduce a novel **Focal-Confidence Loss**, which integrates both class-level prediction difficulty and pixel-level label reliability. It addresses two core challenges: noisy pseudo-labels and severe class imbalance in historical segmentation. For every blockBin SAM The confidence and input classes for pseudo-labels are defined as follows:

$$\text{Pseudo}(B), \text{Conf}(B) = \begin{cases} (c^*, p_{c^*}(B)), & \text{if } p_{c^*}(B) \geq \tau_{\text{high}} \\ (\text{ignore}, 0), & \text{if } p_{c^*}(B) < \tau_{\text{low}} \\ (c, \{p_c(B)\}_{c=1}^C), & \text{otherwise} \end{cases} \quad (1)$$

where $p_c(B)$ is the proportion of class c in block B , and $c^* = \arg \max_c p_c(B)$, class c is predicted by the teacher model. Finally, the loss is modulated by mechanisms to focus training on trustworthy and challenging areas. The full formulation of the Focal-Confidence Loss is as follows:

$$\mathcal{L}_{\text{focal-confi}} = \frac{1}{N} \sum_i \left[\alpha \cdot (1 - \bar{p}_{y_i})^\gamma \cdot \text{CE}(x_i, y_i) \cdot c_i^\beta \right] \quad (2)$$

Where: $\text{CE}(x_i, y_i)$ is the cross-entropy loss between prediction x_i and pseudo label y_i . \bar{p}_{y_i} is the average softmax probability of class y_i across the batch, representing class confidence. c_i is the consistency-based confidence score ($\text{Conf}(B)$) for pixel i . γ and β are focusing parameters to control sensitivity (e.g., $\gamma = 2, \beta = 0.5$). α is a balancing factor.

5 Experiments

5.1 Experimental Setups

Evaluation Metrics. We adopt two standard metrics for unsupervised segmentation: mean Intersection over Union (mIoU) and Overall Accuracy (Acc).

Comparison Methods. We compare Urban1960SatUSM with representative baselines in two categories:

1) Unsupervised clustering methods that rely solely on features extracted by DINO[3] or DINOv2; 2) Self-supervised semantic segmentation frameworks built upon DINO or DINOv2[22], including STEGO[12], HP[28], EAGLE[18], and Primaps-EM[11]. Please refer to the supplementary material for more details about the implementation details.

5.2 Experimental Results on Urban1960SatBench

As shown in Tab. 2 and Tab. 1 in the supplementary material, Urban1960SatUSM achieves state-of-the-art performance in most cases across the Urban1960SatBench benchmark (including both

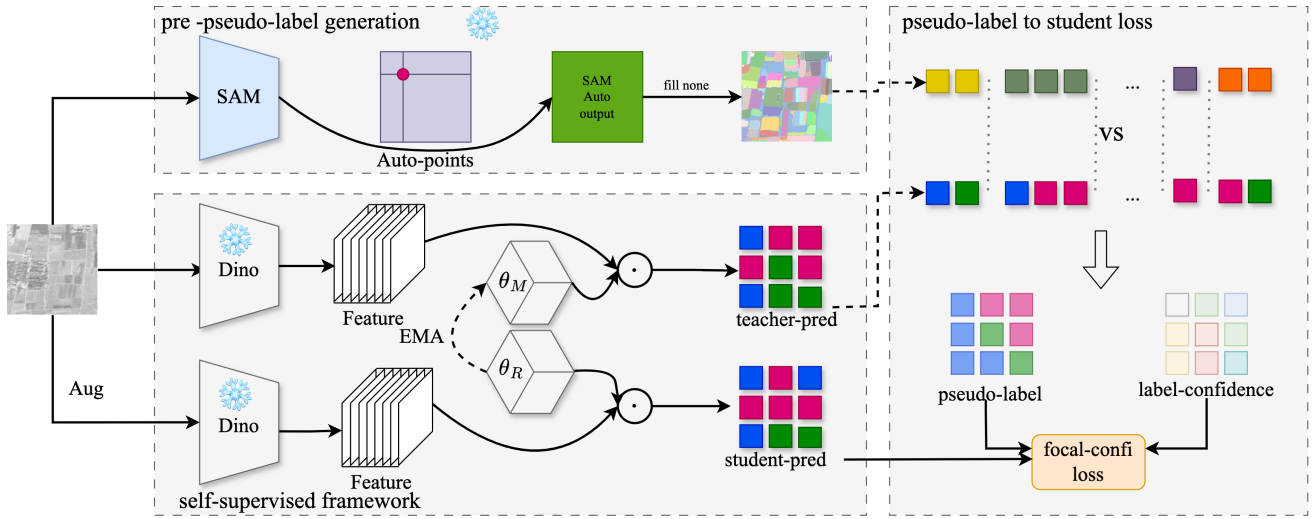


Figure 4: Architecture of Urban1960SatUSM, an unsupervised segmentation model designed for urban scene analysis

Table 2: Performance comparison on the Urban1960SatSS dataset between Urban1960SatUSM(Ours) and existing unsupervised semantic segmentation methods, measured by Accuracy and mean IoU (in %) for both unsupervised and supervised probing.

Method	Backbone	Unsupervised		Supervised	
		mIoU	Acc	mIoU	Acc
Dino[3]	DINO ViT - S/8	25.2	62.5	65.9	91.0
+ STEGO [12]	DINO ViT - S/8	18.7	74.9	18.7	74.9
+HP [28]	DINO ViT - S/8	26.7	58.6	32.8	63.0
+ EAGLE [18]	DINO ViT - S/8	31.3	62.4	60.0	90.0
+ PriMaPs - EM [11]	DINO ViT - S/8	22.7	74.6	65.6	91.2
+ Urban1960SatUSM	DINO ViT - S/8	20.5	70.7	65.6	91.2
Dino[3]	DINO ViT - B/8	25.1	48.2	63.9	90.3
+ STEGO [12]	DINO ViT - B/8	35.4	73.1	59.4	90.7
+HP [28]	DINO ViT - B/8	24.3	73.0	51.9	81.6
+ EAGLE [18]	DINO ViT - B/8	26.4	52.0	61.6	91.2
+ PriMaPs - EM [11]	DINO ViT - B/8	49.6	71.7	68.8	92.7
+ Urban1960SatUSM	DINO ViT - B/8	57.8	78.6	68.8	92.8
Dinov2[22]	DINOv2 ViT - S/14	36.4	55.4	66.0	92.1
+ PriMaPs - EM [11]	DINOv2 ViT - S/14	33.4	57.7	63.9	91.7
+ Urban1960SatUSM	DINOv2 ViT - S/14	38.6	71.4	66.5	92.2
Dinov2[22]	DINOv2 ViT - B/14	40.5	71.4	62.5	89.6
+ PriMaPs - EM [11]	DINOv2 ViT - B/14	34.0	70.0	62.2	89.3
+ Urban1960SatUSM	DINOv2 ViT - B/14	46.4	82.1	64.9	92.6

Urban1960SatSS and Urban1960SatISP) under unsupervised learning settings. This demonstrates the robustness and generalizability of our approach in tackling complex urban nighttime scene understanding tasks. Notably, Urban1960SatUSM significantly outperforms most baselines on mIoU and Accuracy, demonstrating precise fine-grained segmentation. For instance, with DINOv2 ViT-B/14, Urban1960SatUSM achieves the highest mIoU of 46.4% and Accuracy of 82.1% in the unsupervised setting on Urban1960SatSS, and reaches 75.0% mIoU and 91.1% Accuracy under unsupervised settings on Urban1960SatISP. When using DINO as the backbone, compared to baseline self-supervised approaches, Urban1960SatUSM

introduces significant gains across all metrics, highlighting its effectiveness in denoising historical Keyhole satellite data under unsupervised settings, especially in handling grayscale input, variable resolution (ranging from 0.6m to 1.8m), and scanning artifacts. When using DINOv2 as the backbone, Urban1960SatUSM also demonstrates superior scalability and adaptability. It consistently improves both mIoU and Accuracy across various configurations, showing robust performance across patch sizes and training setups. These results underscore Urban1960SatUSM’s ability to fully leverage the representational power of DINO and integrate the fine-grained segmentation capabilities of SAM, especially for large-scale urban imagery. Please refer to supplementary material for the ablation study.

To further evaluate the segmentation accuracy, Fig. 1 in the supplementary material presents visual comparisons on representative urban areas. These findings confirm the superior capability of our framework in processing complex remote sensing modalities, and lay a solid foundation for large-scale spatiotemporal segmentation tasks across different regions and years. This supports downstream tasks like urban planning and assessing infrastructure impact on economic development.

6 Conclusion and Future Work

We present Urban1960SatBench, the first benchmark dataset for semantic segmentation of historical Keyhole satellite imagery, and propose Urban1960SatUSM, a self-supervised framework that combines frozen feature extractors with SAM-generated pre-pseudo-labels. Experiments show that Urban1960SatUSM outperforms existing unsupervised methods on both binary and multi-class tasks. Looking ahead, we identify several future directions to advance historical urban analytics: (1) **Temporal expansion across decades**. Extending Urban1960SatBench to the 1980s enables long-term urban morphology analysis. (2) **Cross-region generalization**. Adapting the framework to global cities supports cross-cultural comparisons in urban studies.

References

- [1] National Aeronautics and Space Administration. 2008. The ASTER image of the Heihe River Basin (2000–2008). <https://dx.doi.org/>
- [2] Faraz Bastani, Rafael Clivatti, Rohan Iyer, Enrico Fini, Rohan Paul, Phillip Marcus, Ananth Ramesh, Michael Maire, Han Chang, Lorenzo Torresani, Deva Ramanan, Nuno Pinto, Emilio Frazzoli, and Abhinav Khosla. 2024. EarthView: A Large Scale Remote Sensing Dataset for Self-Supervision. *arXiv preprint arXiv:2501.08111* (2024).
- [3] Mathilde Caron, Hugo Touvron, Ishan Misra, Hervé Jégou, Julien Mairal, Piotr Bojanowski, and Armand Joulin. 2021. Emerging Properties in Self-Supervised Vision Transformers. In *Proceedings of the International Conference on Computer Vision (ICCV)*.
- [4] Dengxin Dai and Wen Yang. 2011. Satellite image classification via two-layer sparse coding with biased image representation. *IEEE Geoscience and Remote Sensing Letters* 8, 1 (2011), 173–176.
- [5] Ajay Dashora, Bharat Lohani, and Javed N Malik. 2007. A repository of earth resource information—CORONA satellite programme. *Current Science* (2007), 926–932.
- [6] Grupo de Inteligencia Computacional (GIC). [n. d.]. Hyperspectral Remote Sensing Scenes. https://www.ehu.es/ccwintco/index.php/Hyperspectral_Remote_Sensing_Scenes. Accessed: 2025-05-27.
- [7] Ilke Demir, Krzysztof Koperski, David Lindenbaum, Guan Pang, Jing Huang, Saikat Basu, Forest Hughes, Devis Tuia, and Ramesh Raskar. 2018. DeepGlobe 2018: A Challenge to Parse the Earth Through Satellite Images. In *Proceedings of the IEEE Conference on Computer Vision and Pattern Recognition (CVPR) Workshops*, 172–181. doi:10.1109/CVPRW.2018.00031
- [8] Steven Foga, Pat L. Scaramuzza, Shunlin Guo, Zhe Zhu, Robert D. Dilley, Timothy Beckmann, Gail L. Schmidt, John L. Dwyer, Michael J. Hughes, and Brian Lau. 2017. Cloud detection algorithm comparison and validation for operational Landsat data products. *Remote Sensing of Environment* 194 (2017), 379–390. doi:10.1016/j.rse.2017.03.026
- [9] Alistair Francis, John Mrziglod, Panagiotis Sidiropoulos, and Jan-Peter Muller. 2020. Sentinel-2 Cloud Mask Catalogue. doi:10.5281/zenodo.4172871
- [10] Olivier Hagolle, Gérard Dedieu, Stefan Auer, Sophie Bontemps, Jordi Inglada, Martin Huc, Daniel Villa Pascual, and Claire Marais-Sicre. 2019. Validation of Copernicus Sentinel-2 Cloud Masks Obtained from MAJA, Sen2Cor, and FMask Processors Using Reference Cloud Masks Generated with a Supervised Active Learning Procedure. *Remote Sensing* 11, 4 (2019), 433. doi:10.3390/rs11040433
- [11] Oliver Hahn, Nikita Araslanov, Simone Schaub-Meyer, and Stefan Roth. 2024. Boosting Unsupervised Semantic Segmentation with Principal Mask Proposals. *Transactions on Machine Learning Research (TMLR)* (2024).
- [12] Mark Hamilton, Zhoulong Zhang, Bharath Hariharan, Noah Snavely, and William T. Freeman. 2022. Unsupervised Semantic Segmentation by Distilling Feature Correspondences. In *International Conference on Learning Representations*. <https://openreview.net/forum?id=SaKO6z6Hl0c>
- [13] Taisei Hanyu, Kashi Yamazaki, Minh Tran, Roy A. McCann, Haitao Liao, Chase Rainwater, Meredith Adkins, Jackson Cothren, and Ngan Le. 2024. AerialFormer: Multi-Resolution Transformer for Aerial Image Segmentation. *Remote Sensing* 16, 16 (2024). doi:10.3390/rs16162930
- [14] M. Joseph Hughes and Daniel J. Hayes. 2014. Automated Detection of Cloud and Cloud Shadow in Single-Date Landsat Imagery Using Neural Networks and Spatial Post-Processing. *Remote Sensing* 6, 6 (2014), 4907–4926. doi:10.3390/rs6064907
- [15] Ronny Hänsch, Jacob Arndt, Dalton Lunga, Matthew Gibb, Tyler Pedelose, Arnold Boedihardjo, Desiree Petrie, and Todd M. Bacastow. 2022. SpaceNet 8 - The Detection of Flooded Roads and Buildings. In *Proceedings of the IEEE/CVF Conference on Computer Vision and Pattern Recognition (CVPR) Workshops*, 1471–1479. https://openaccess.thecvf.com/content/CVPR2022W/EarthVision/papers/Hansch_SpaceNet_8_-_The_Detection_of_Flooded_Roads_and_Buildings_CVPRW_2022_paper.pdf
- [16] Shunping Ji, Shiqing Wei, and Meng Lu. 2019. Fully Convolutional Networks for Multisource Building Extraction from an Open Aerial and Satellite Imagery Data Set. *IEEE Transactions on Geoscience and Remote Sensing* 57, 1 (2019), 574–586. doi:10.1109/TGRS.2018.2858817
- [17] Shunping Ji, Dawen Yu, Chaoyong Shen, Weile Li, and Qiang Xu. 2020. Landslide detection from an open satellite imagery and digital elevation model dataset using attention boosted convolutional neural networks. *Landslides* 17, 6 (2020), 1337–1352. doi:10.1007/s10346-020-01353-2
- [18] Chanyoung Kim, Woojung Han, Dayun Ju, and Seong Jae Hwang. 2024. EAGLE: Eigen Aggregation Learning for Object-Centric Unsupervised Semantic Segmentation. In *Proceedings of the IEEE/CVF Conference on Computer Vision and Pattern Recognition (CVPR)*, 3523–3533.
- [19] Bertrand Le Saux, Naoto Yokoya, Ronny Hänsch, and Saurabh Prasad. 2018. 2018 IEEE GRSS Data Fusion Contest: Multimodal Land Use Classification [Technical Committees]. *IEEE Geoscience and Remote Sensing Magazine* 6, 1 (March 2018), 52–54. doi:10.1109/MGRS.2018.2798161
- [20] Xianping Ma, Qianqian Wu, Xingyu Zhao, Xiaokang Zhang, Man-On Pun, and Bo Huang. 2024. SAM-Assisted Remote Sensing Imagery Semantic Segmentation With Object and Boundary Constraints. *IEEE Transactions on Geoscience and Remote Sensing* 62 (2024), 1–16. doi:10.1109/TGRS.2024.3443420
- [21] S. Mohajerani and P. Saeedi. 2020. Cloud-Net+: A Cloud Segmentation CNN for Landsat 8 Remote Sensing Imagery Optimized with Filtered Jaccard Loss Function. *arXiv* 2001.08768.
- [22] Maxime Quab, Timothée Darcet, Théo Moutakanni, Huy V. Vo, Marc Szafraniec, Vasil Khalidov, Pierre Fernandez, Daniel HAZIZA, Francisco Massa, Alaaeldin El-Nouby, Mido Assran, Nicolas Ballas, Wojciech Galuba, Russell Howes, Po-Yao Huang, Shang-Wen Li, Ishan Misra, Michael Rabbat, Vasu Sharma, Gabriel Synnaeve, Hu Xu, Herve Jegou, Julien Mairal, Patrick Labatut, Armand Joulin, and Piotr Bojanowski. 2024. DINOv2: Learning Robust Visual Features without Supervision. *Transactions on Machine Learning Research* (2024). <https://openreview.net/forum?id=a68SU6t2Ft> Featured Certification.
- [23] P. Potapov et al. 2022. Long-Term Monitoring of Land-Use and Land-Cover Changes. *Frontiers in Remote Sensing* (2022). https://www.frontiersin.org/journals/remote-sensing/articles/10.3389/frsen.2022.856903/full?utm_source=chatgpt.com
- [24] Xiaoman Qi, Panpan Zhu, Yuebin Wang, Liqiang Zhang, Junhuan Peng, Mengfan Wu, Jialong Chen, Xudong Zhao, Ning Zang, and P Takis Mathiopoulos. 2020. MLRSNet: A multi-label high spatial resolution remote sensing dataset for semantic scene understanding. *ISPRS Journal of Photogrammetry and Remote Sensing* 169 (2020), 337–350.
- [25] Franz Rottensteiner. 2013. Isprs test project on urban classification and 3d building reconstruction: Evaluation of building reconstruction results. *Technical report* (2013).
- [26] Luigi Russo, Francesco Mauro, Alessandro Sebastianelli, Paolo Gamba, and Silvia Liberata Ullo. 2024. SEN12-WATER: A New Dataset for Hydrological Applications and its Benchmarking. *arXiv preprint arXiv:2409.17087* (2024). doi:10.48550/arXiv.2409.17087
- [27] Sudipan Saha, Begüm Demir, and Volker Markl. 2017. Multimodal Change Detection with Weakly Supervised Learning for Disaster Response. In *2017 20th International Conference on Information Fusion (Fusion)*, 1–8. doi:10.23919/ICIF.2017.8009841
- [28] Hyun Seok Seong, WonJun Moon, SuBeen Lee, and Jae-Pil Heo. 2023. Leveraging hidden positives for unsupervised semantic segmentation. In *Proceedings of the IEEE/CVF conference on computer vision and pattern recognition*, 19540–19549.
- [29] Aysim Toker, Lukas Kondmann, Mark Weber, Marvin Eisenberger, Camero Andres, Jingliang Hu, Ariadna Hoderlein, Caglar Senaras, Timothy Davis, Daniel Cremers, Giovanni Marchisio, Xiaoxiang Zhu, and Laura Leal-Taixe. 2022. DynamicEarthNet: Daily Multi-Spectral Satellite Dataset for Semantic Change Segmentation. In *Proceedings of the IEEE/CVF Conference on Computer Vision and Pattern Recognition (CVPR)*.
- [30] Xin-Yi Tong, Gui-Song Xia, Qikai Lu, Huanfeng Shen, Shengyang Li, Shucheng You, and Liangpei Zhang. 2020. Land-cover classification with high-resolution remote sensing images using transferable deep models. *Remote Sensing of Environment* 237 (2020), 111322.
- [31] UnitedNations. 2015. Transforming our world: the 2030 Agenda for Sustainable Development. *United Nations: New York, NY, USA* (2015).
- [32] U.S. Geological Survey. 2016. L8 SPARCS Cloud Validation Masks. doi:10.5066/F7FB5146
- [33] Michele Volpi and Vittorio Ferrari. 2015. Semantic Segmentation of Urban Scenes by Learning Local Class Interactions. In *Proceedings of the IEEE Conference on Computer Vision and Pattern Recognition (CVPR) Workshops*, 1–9. doi:10.1109/CVPRW.2015.7301377
- [34] Junjue Wang, Zhuo Zheng, Ailong Ma, Xiaoyan Lu, and Yanfei Zhong. 2021. LoveDA: A Remote Sensing Land-Cover Dataset for Domain Adaptive Semantic Segmentation. In *Proceedings of the Neural Information Processing Systems Track on Datasets and Benchmarks*, J. Vanschoren and S. Yeung (Eds.), Vol. 1. Curran Associates, Inc. https://datasets-benchmarks-proceedings.neurips.cc/paper_files/paper/2021/file/4e732ced3463d06de0ca9a15b6153677-Paper-round2.pdf
- [35] Gui-Song Xia, Wen Yang, Julie Delon, Yann Gousseau, Hong Sun, and Henri Maître. 2010. Structural high-resolution satellite image indexing. In *ISPRS Technical Commission VII Symposium—100 Years ISPRS*, 298–303.
- [36] Danlin Yu and Chuanglin Fang. 2023. Urban Remote Sensing with Spatial Big Data: A Review and Renewed Perspective of Urban Studies in Recent Decades. *Remote Sensing* 15, 5 (2023), 1307. doi:10.3390/rs15051307
- [37] Shuai Yuan, Runmin Dong, Juepeng Zheng, Wenzhao Wu, Lixian Zhang, Weijia Li, and Haohuan Fu. 2020. Long time-series analysis of urban development based on effective building extraction. In *Geospatial Informatics X*, Vol. 11398. SPIE, 192–199.
- [38] Hao Zhang, Feng Li, Xueyan Zou, Shilong Liu, Chunyuan Li, Jianwei Yang, and Lei Zhang. 2023. A Simple Framework for Open-Vocabulary Segmentation and Detection. In *Proceedings of the IEEE/CVF International Conference on Computer Vision (ICCV)*, 1020–1031.
- [39] Lixian Zhang, Zhehao Ren, Bin Chen, Peng Gong, Bing Xu, and Haohuan Fu. 2024. A prolonged artificial nighttime-light dataset of China (1984–2020). *Scientific*

- Data* 11, 1 (2024), 414.
- [40] Lixian Zhang, Shuai Yuan, Runmin Dong, Juepeng Zheng, Bin Gan, Dengmao Fang, Yang Liu, and Haohuan Fu. 2024. SWCARE: Switchable learning and connectivity-aware refinement method for multi-city and diverse-scenario road mapping using remote sensing images. *International Journal of Applied Earth Observation and Geoinformation* 127 (2024), 103665. doi:10.1016/j.jag.2024.103665
- [41] Mi Zhang, Xiangyun Hu, Like Zhao, Ye Lv, Min Luo, and Shiyan Pang. 2017. Learning Dual Multi-Scale Manifold Ranking for Semantic Segmentation of High-Resolution Images. *Remote Sensing* 9, 5 (2017), 500. doi:10.3390/rs9050500
- [42] Xin Zhang, Yu Liu, Yuming Lin, Qingmin Liao, and Yong Li. 2024. UV-SAM: Adapting Segment Anything Model for Urban Village Identification. *Proceedings of the AAAI Conference on Artificial Intelligence* 38, 20 (Mar. 2024), 22520–22528. doi:10.1609/aaai.v38i20.30260
- [43] Tianfei Zhou, Wang Xia, Fei Zhang, Boyu Chang, Wenguan Wang, Ye Yuan, Ender Konukoglu, and Daniel Cremers. 2024. Image segmentation in foundation model era: A survey. *arXiv preprint arXiv:2408.12957* (2024).
- [44] Xueyan Zou*, Zi-Yi Dou*, Jianwei Yang*, Zhe Gan, Linjie Li, Chunyuan Li, Xiyang Dai, Jianfeng Wang, Lu Yuan, Nanyun Peng, Lijuan Wang, Yong Jae Lee*, and Jianfeng Gao*. 2022. Generalized Decoding for Pixel, Image and Language. (2022).
- [45] Xueyan Zou, Jianwei Yang, Hao Zhang, Feng Li, Linjie Li, Jianfeng Wang, Lijuan Wang, Jianfeng Gao, and Yong Jae Lee. 2023. Segment Everything Everywhere All at Once. In *Advances in Neural Information Processing Systems*, A. Oh, T. Naumann, A. Globerson, K. Saenko, M. Hardt, and S. Levine (Eds.), Vol. 36. Curran Associates, Inc., 19769–19782. https://proceedings.neurips.cc/paper_files/paper/2023/file/3ef61f7e4afacf9a2c5b71c726172b86-Paper-Conference.pdf

A Supplementary Experimental Results

Table 3: Performance comparison on the Urban1960SatISP dataset between Urban1960SatUSM(Ours) and existing unsupervised semantic segmentation methods, measured by Accuracy and mean IoU (in %) for both unsupervised and supervised probing.

Method	Backbone	Unsupervised		Supervised	
		mIoU	Acc	mIoU	Acc
Dino[3]	DINO ViT - S/8	43.8	71.4	80.1	92.9
+ STEGO [12]	DINO ViT - S/8	39.9	79.7	40.1	79.7
+HP [28]	DINO ViT - S/8	22.4	60.4	25.8	68.3
+ EAGLE [18]	DINO ViT - S/8	57.4	76.1	82.2	93.8
+ PriMaPs - EM [11]	DINO ViT - S/8	43.2	81.8	81.2	93.2
+ Urban1960SatUSM	DINO ViT - S/8	52.7	81.2	80.1	92.9
Dino[3]	DINO ViT - B/8	57.8	77.0	83.1	94.1
+ STEGO [12]	DINO ViT - B/8	74.0	88.9	78.4	92.3
+HP [28]	DINO ViT - B/8	19.0	53.1	35.6	73.3
+ EAGLE [18]	DINO ViT - B/8	39.0	62.9	78.6	93.0
+ PriMaPs - EM [11]	DINO ViT - B/8	60.4	79.0	83.1	94.1
+ Urban1960SatUSM	DINO ViT - B/8	61.5	80.1	83.1	94.0
Dinov2[22]	DINOv2 ViT - S/14	62.2	81.0	82.0	93.7
+ PriMaPs - EM [11]	DINOv2 ViT - S/14	57.3	77.6	82.7	93.9
+ Urban1960SatUSM	DINOv2 ViT - S/14	75.3	91.0	81.8	93.7
Dinov2[22]	DINOv2 ViT - B/14	70.7	87.2	79.0	92.0
+ PriMaPs - EM [11]	DINOv2 ViT - B/14	66.8	85.4	82.3	93.5
+ Urban1960SatUSM	DINOv2 ViT - B/14	75.0	91.1	80.6	93.6